Danming Zhong[1]
Key Laboratory of Soft Machines and Smart Devices of Zhejiang Province, Department of Engineering Mechanics, Zhejiang University, Hangzhou 310027, China
e-mail: danmingzhong@163.com

Junjie Liu[1]
Key Laboratory of Soft Machines and Smart Devices of Zhejiang Province, Department of Engineering Mechanics, Zhejiang University, Hangzhou 310027, China
e-mail: 1563416987@qq.com

Yuhai Xiang
Key Laboratory of Soft Machines and Smart Devices of Zhejiang Province, Department of Engineering Mechanics, Zhejiang University, Hangzhou 310027, China
e-mail: xiangyuhai@zju.edu.cn

Tenghao Yin
Key Laboratory of Soft Machines and Smart Devices of Zhejiang Province, Department of Engineering Mechanics, Zhejiang University, Hangzhou 310027, China
e-mail: yinth@zju.edu.cn

Wei Hong[2]
Department of Mechanics and Aerospace Engineering, Southern University of Science and Technology, Shenzhen, Guangdong 518055, China
e-mail: hongw@sustc.edu.cn

Honghui Yu
Department of Mechanical Engineering, The City College of New York, New York, NY 10031
e-mail: yu@ccny.cuny.edu

Shaoxing Qu[2]
Key Laboratory of Soft Machines and Smart Devices of Zhejiang Province, Department of Engineering Mechanics, Zhejiang University, Hangzhou 310027, China
e-mail: squ@zju.edu.cn

Wei Yang
Key Laboratory of Soft Machines and Smart Devices of Zhejiang Province, Department of Engineering Mechanics, Zhejiang University, Hangzhou 310027, China
e-mail: yangw@zju.edu.cn

Effect of Partition on the Mechanical Behaviors of Soft Adhesive Layers

A soft adhesive layer bonded between two rigid substrates, which are being pulled apart, may exhibit diverse instability phenomena before failure, such as cavitation, fingering, and fringe instability. In this study, by subdividing the soft layers into different numbers of disconnected smaller parts, we achieve desired instability modes and mechanical responses of the layer. The partition process not only retains the monotonicity on the tensile curve but also tunes the modulus and stretchability of the adhesive layer. Meanwhile, cavitation in layers of large aspect ratios is suppressed, and the hysteresis during cyclic loading is reduced. This study provides a guideline for the structural design of soft joints and adhesive layers. [DOI: 10.1115/1.4042764]

Keywords: adhesive, instability, partition

[1]Danming Zhong and Junjie Liu contributed equally to this work.
[2]Corresponding authors.

Contributed by the Applied Mechanics Division of ASME for publication in the JOURNAL OF APPLIED MECHANICS. Manuscript received January 1, 2019; final manuscript received February 3, 2019; published online March 16, 2019. Assoc. Editor: Yonggang Huang.

1 Introduction

Soft adhesive layers, which could also be found in living systems [1,2], are widely used in engineering applications such as sealants, mechanical insulators, and soft robotics [3–5]. When a soft adhesive layer bonded between two rigid substrates is subjected to through thickness tension, various instabilities such as cavitation, fingering, and fringe can occur depending on the geometric constraints by the substrates and the material properties of the layer [6–14]. These instabilities can significantly affect the mechanical responses of the adhesive layer [3]. Moreover, they can lead to damages in the form of interfacial fracture or cohesive failure in the adhesive layer [13].

If the interface between the soft adhesive and the rigid substrate is weak, the adhesive layer may partially debond from the rigid substrate, and the delaminated interface undulates regularly due to interfacial instability [15–17]. Animangsu and Chaudhury [18] observed instabilities in the form of fingers and bubbles along the interface between a thin confined film and its covering plate and pointed out that the characteristic length of the interfacial instabilities depend only on the film thickness. Webber et al. [19] found that the lateral constraint has a huge impact on the interfacial instability of the confined soft layer under tension. When the resistance to interfacial cracks is high enough, delamination arrests but bulk instabilities arise. For an adhesive layer with larger elastic modulus and lateral constraint, cavitation is preferred over other instability modes [20]. By treating cavitation as an elastic instability problem, Dollhofer et al. [21] pointed out that for neo-Hookean material, surface energy may have a large effect on the nucleation and the growth of a cavity. According to the Gent and Lindley's [22] theoretical prediction, a pre-existing cavity under remote hydrostatic tension would expand monotonically as the load increases and explode when the hydrostatic tension reaches $5E/6$, with E being the elastic modulus. Dollhofer et al. [21] and Chiche et al. [23] took into account the

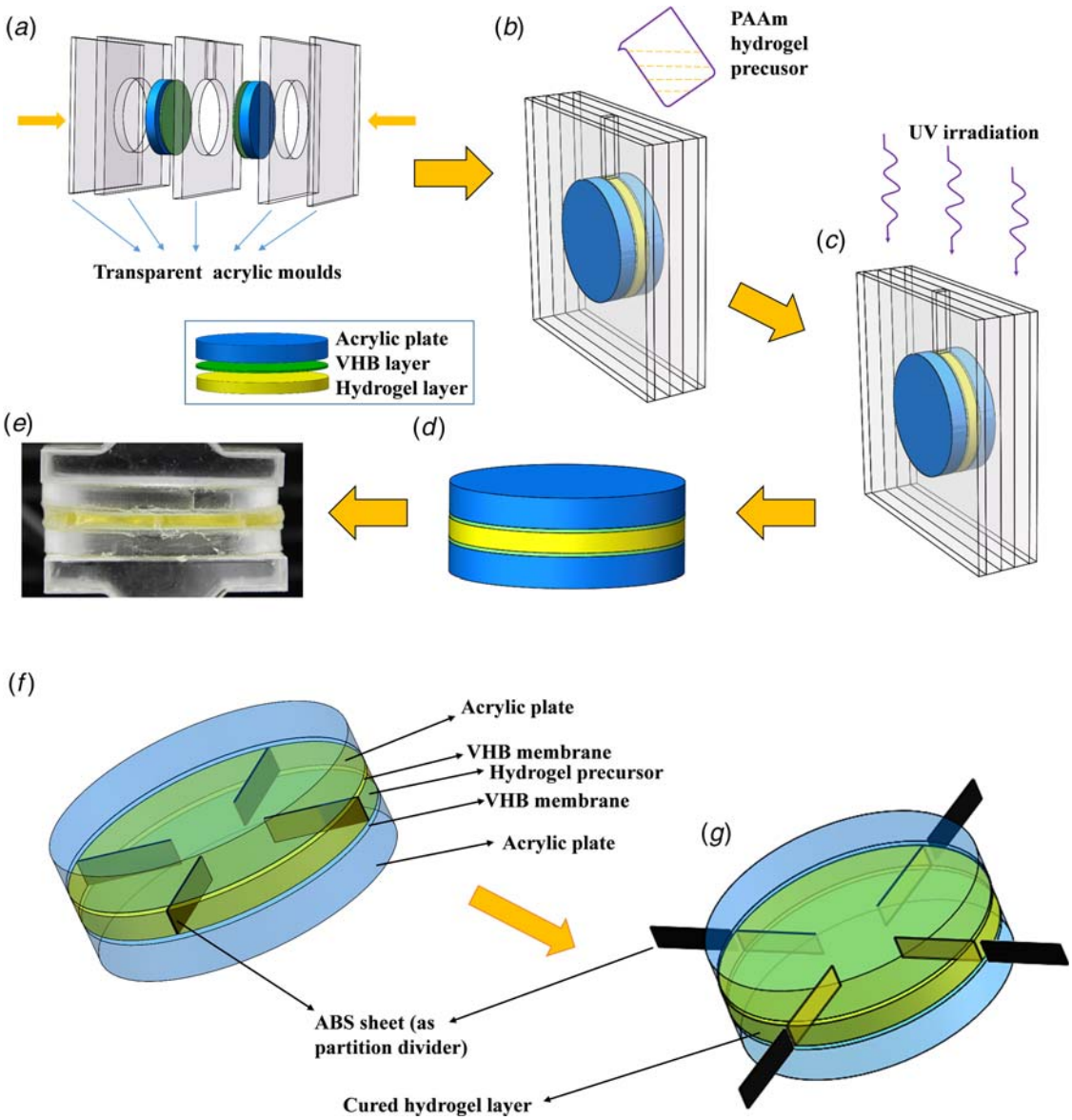

Fig. 1 Procedure for specimen preparation. (*a*) Transparent acrylic molds, acrylic plates, and VHB membranes are cut into specific sizes. (*b*) The components are assembled into a mold with a cylindrical space, which is later filled with a PAAm hydrogel precursor. (*c*) The hydrogel precursor is cured under UV light for 1 h. (*d*) Schematic and (*e*) photograph of the final specimen. (*f*) ABS sheets as dividers with certain size and quantity is placed between two acrylic substrates, and then the hydrogel precursor is poured into the space. (The outside acrylic molds are not shown for clarity.) (*g*) After curing the hydrogel, the partition dividers are pulled out carefully. In this case, the number of partitions is four, and the length of partition divider is two-third of the radius.

additional stress field induced by surface tension and concluded that for an adhesive layer of a large relative surface tension (γ/ER_0, where γ is the surface energy of the material and R_0 is the size of the initial defect/cavity), there exists a peak stress at which the cavity becomes elastically unstable [24,25] before the final failure. By realizing that a cavity may grow inelastically before reaching the elastic instability limit, Pourmodheji et al. [26] analyzed the driving force and the resistance of the inelastic cavity growth and found a characteristic length. When the cavity size is smaller than the characteristic length, the critical stress is size independent, and the cavity grows inelastically by omnidirectional expansion at a constant hydrostatic stress until the characteristic length is reached. After that, it grows by cracking along a plane.

For an adhesive layer with a smaller elastic modulus and lateral constraint, fingering instability may precede cavitation. Shull et al. [27] observed reversible bulk fingering instability in purely elastic materials subjected to cyclical tensile loadings. Biggins et al. [28] put forward a simple zero-dimensional model to explain how bulk fingers could reduce the total shear energy and predicted the wavelength and threshold of the fingering instability. Saintyves et al. [29] demonstrated elastic fingering in a bulk polyacrylamide (PAAm) gel confined in a Hele-Shaw cell. Recently, Lin et al. [12] calculated the critical stretch and stress for the onsets of fingering and fringe instabilities by adopting a perturbation method. They provided a phase diagram of different instabilities.

Although substantial investigations have been carried out on the instabilities in the confined soft adhesive layer subjected to uniaxial tension, few of them have considered to alter the instability modes, as well as the mechanical responses of adhesive layers. In this paper, we propose a method to tune the instability and the corresponding mechanical responses of a soft adhesive layer by partitioning the adhesive layer. By using this method, one can convert the stress–stretch curve of the soft adhesive layer from a nonmonotonous relationship to a monotonous one and eliminate the snap-through phenomenon, which is important for the reliability of the adhesive layer under force-controlled loading. Furthermore, a partitioned adhesive layer may undergo larger deformation before failure, and consequently, the stretchability may be tuned. Moreover, the area of the hysteresis loop decreases after partitioning, indicating less energy dissipation.

This paper consists of the following parts. Section 2 describes the details of the experimental setup and the numerical simulation. Section 3 presents the experimental and numerical results. Section 4 provides the discussions, followed by the conclusions in Sec. 5.

2 Experiment and Numerical Simulation

2.1 Specimen Preparation. In each test, the PAAm hydrogel layer, used as the soft adhesive layer, is confined between two rigid circular acrylic plates. The specimens are prepared by casting, and the detailed procedure is shown in Figs. 1(*a*)–1(*e*). First, two circular acrylic plates with diameter 30 mm (or 50 mm) and thickness 4 mm are placed in a mold, and the surface of the acrylic plate is covered by a VHB 4905 (3 M) tape to enhance the bonding between the hydrogel adhesive layer and the acrylic plates. Considering that the thickness of VHB 4905 layer (0.5 mm) is about one-fifth of that of the hydrogel layer (2.6 mm) and the shear modulus of VHB 4905 (54 kPa) [30] is one order of magnitude higher than that of the hydrogel (3.6 kPa) used in this paper, we neglect the effect of the VHB 4905 layer on the deformation of the hydrogel layer. Second, a PAAm hydrogel precursor is poured into the mold, filling the space between the acrylic plates. Finally, the mold with hydrogel precursor is exposed to UV light (Ultraviolet Crosslinker, CL-1000, USA) for 1 h to cure the hydrogel. The PAAm hydrogel precursor is a mixture of 10 ml 13 wt. % acrylamide (Aladdin A108465), 0.1 ml 1.09 wt. % *N*,*N*-methylenebisacrylamide (Aladdin M104027) as a crosslinker, 0.1 ml 10.9 wt. % ammonium persulphate (Aladdin A112448) as an initiator, and 1 μl *N*,*N*,*N*′,*N*′-tetramethylethylenediamine (Aladdin T105498) as an accelerator. The thickness of the soft adhesive layer (H) is set at 2.6 mm and the diameter (a) is taken to be 30 mm and 50 mm, with aspect ratios ($\alpha = a/H$) of about 12 and 20, respectively.

To partition the adhesive layer, we use acrylonitrile butadiene styrene (ABS) sheets with thickness of 0.2 mm to divide the space between the rigid substrates, as shown in Fig. 1(*f*). We should point out that the VHB membrane is sticky, so we stick the ABS dividers on the surface of VHB membrane first, and the following process is the same as the process without dividers. The adhesion between ABS dividers and VHB membrane is strong enough to fix the dividers. The ABS sheets are used directly without any special treatment, and the interface between ABS sheets and cured hydrogel is weak. Therefore, pulling out the sheets will not cause obvious damage of the surrounding hydrogel. After curing the hydrogel, we pull the ABS sheets out, and the final specimen is shown in Fig. 1(*g*). The adhesive layers are partitioned in this way with different numbers and sizes. For example, for the adhesive layer shown in Fig. 1(*g*), the number of partitions is four and the length of each partition divider is two-third of the radius.

2.2 Specimen Tensile Testing. The as-prepared specimens are stretched on a universal material testing machine (Instron 5944, USA). The bottom acrylic substrate of each specimen is fixed, whereas the top acrylic substrate is pulled upward at a constant speed of 10 mm/min. We recorded the grip displacement and the reaction force during the experiment. We recorded in situ the instability evolution of the hydrogel adhesive layer from the bottom view of the specimen by using a CCD camera (Nikon D7200, Japan). To do that conveniently, we placed a mirror under the specimen at 45 deg from the vertical direction.

2.3 Numerical Simulation. We use ABAQUS/Explicit to carry out the numerical simulation on the mechanical response and instability behaviors of the soft adhesive layer under tensile loading. We choose a neo-Hookean constitutive model to describe the hyperelastic behavior of the material, and the shear modulus in the model is obtained by fitting the uniaxial tension data. The bulk modulus is set as 2000 times of the shear modulus to capture the incompressibility of the material. A 3D continuum element with reduced integration, C3D8R, is adopted, and the mesh size is bounded above by one-tenth of the hydrogel layer thickness to ensure accuracy. The geometric dimensions, boundary conditions, loading condition, and the number and size of partitions are the same as that in the experiments. Perfect bonding is assumed on all interfaces. Symmetry of the structure is used to reduce computation.

3 Results

Figure 2(*a*) shows the nominal stress–stretch curves of the soft adhesive layers (aspect ratio $\alpha = 12$) under various numbers of partitions. The stretch is defined as the deformed thickness divided by the initial thickness. The nominal stress is defined as the tensile force divided by the initial cross-sectional area. The circles correspond to the experimental results, and the solid curves correspond to the simulation. Two sets of data agree well with each other. Figure 2(*b*) shows the fracture stretches and the facture works (area encircled by stress–stretch curve × adhesive layer's original thickness) of the soft adhesive layers under various numbers of partitions. Figure 2(*c*) shows the photographs taken from the bottom view of the adhesive layers at different stretches, corresponding to the curves in Fig. 2(*a*). The instabilities of the hydrogel adhesive layers can be easily recognized from these photographs. Figure 2(*d*) illustrates the instability morphologies obtained by the simulation, which agree well with the experimental photographs. The stress–stretch curve of the nonpartitioned adhesive layer shows an obvious peak. Image A1 describes the deformation of adhesive layer at stretch $\lambda = 1.2$ when no instability occurs. The adhesive layer is further extended to a stretch about $\lambda = 1.4$ (as shown in image A2) and several fingers appear suddenly, corresponding to the stress peak. Under further pulling, fingers gradually propagate

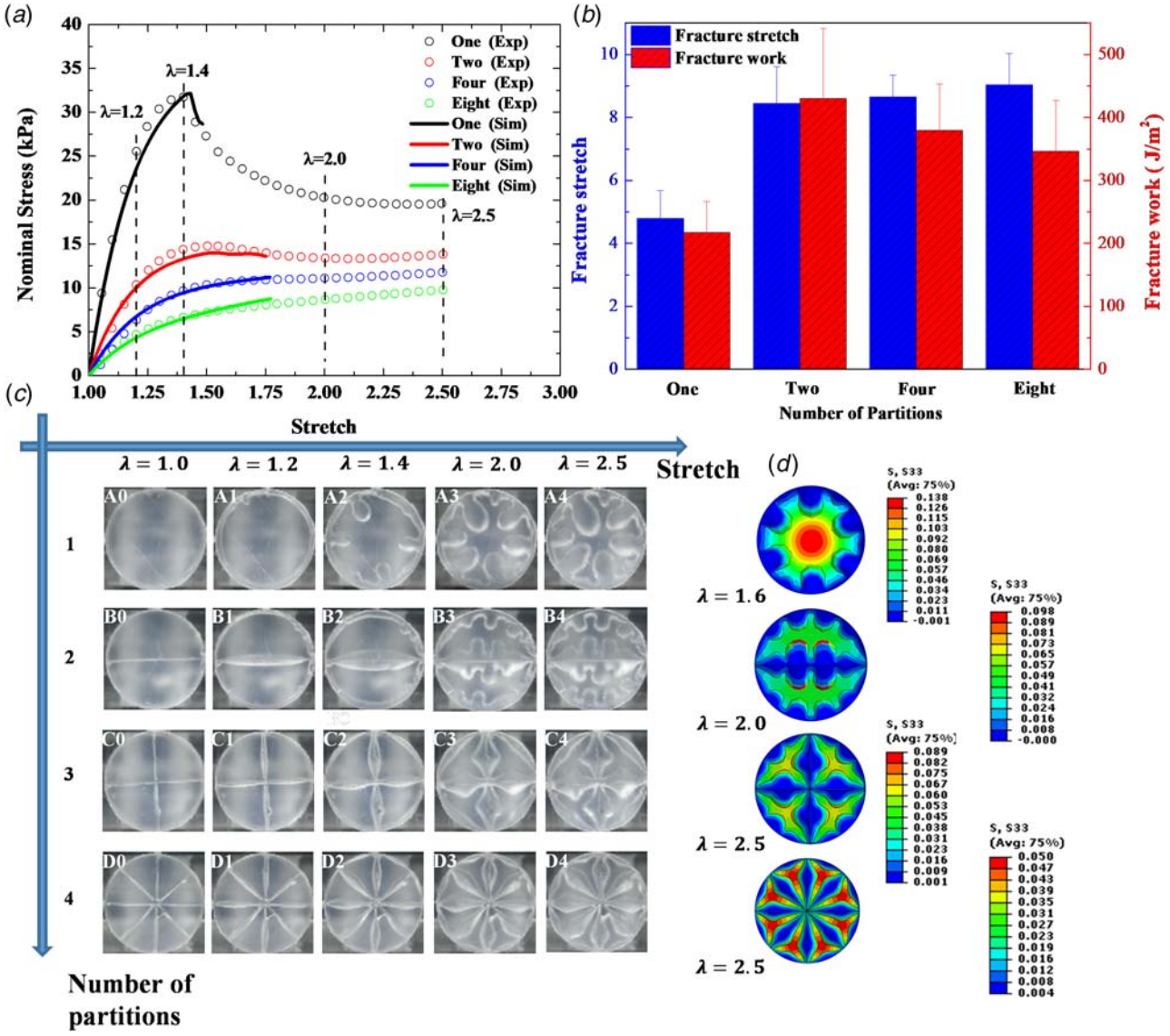

Fig. 2 Mechanical responses of soft adhesive layers (aspect ratio $\alpha = 12$) with various numbers of partitions. (*a*) Nominal stress–stretch curves of the adhesive layers. The circles are obtained from experiments, and the solid curves from simulations. (*b*) Fracture stretches and fracture works of the adhesive layers with various numbers of partitions. (c) Photographs taken from the bottom of the adhesive layers corresponding to the indicated stretches in (*a*). (*d*) Simulated instability morphologies at various numbers of partitions.

into the center of the layer, as shown in image A3. When the adhesive layer is stretched to $\lambda = 2.5$, the fingers are stabilized, and the stress–stretch curve resumes an elasticity-dominated rising tendency.

For the adhesive layer divided into two parts (images B0–B4), a stress peak appears at stretch $\lambda = 1.5$. Compared with the stress–stretch curve of the nonpartitioned adhesive layer, the peak stress drops from 32 kPa to 15 kPa, and the critical stretch at which the layer buckles elevates from 1.4 to 1.5. When the adhesive layer is partitioned into four parts (images C0–C4), fingers propagate into the layer, but no stress peak appears on the stress–stretch curve. A stress plateau can be found from stretch $\lambda = 1.7$ to stretch $\lambda = 2.0$, followed by an increasing stress again. We further increase the numbers of partitions to eight (images D0–D4), and the experiment gives a monotonically increasing stress–stretch curve. Evidently, the instability morphologies and mechanical responses can be adjusted by partitioning the adhesive layers. The overall stiffness decreases with the increasing of numbers of partitions, not only because of the reduction in cross-sectional area but also because of the less effective lateral constraints on smaller partitions. Moreover, the first peak on the stress–stretch curve decreases with the numbers of partitions and vanishes on samples with four or more partitions. It is believed that the gaps between neighboring partitions serve as the nuclei of the fingering instability, which lowers the initiation stress. It is also found that the structure becomes more stretchable when partitioned. The fracture stretch increases significantly when the soft adhesive layer is partitioned into two parts, but further increase in the numbers of partitions only increases the fracture stretch slightly. The fracture work doubles when the layer is divided into two parts and decreases slightly with the further increasing of partition number. Here, for the adhesive layer divided into several parts, each part fractures at different stretch, and the stretch where the first fracture happens is defined as the fracture stretch.

Experiments are also carried out to study the effect of partition number on the mechanical behavior of an adhesive layer with higher aspect ratio ($\alpha = 20$), and similar conclusions can be drawn. For a nonpartitioned adhesive layer, both cavitation and fingering instabilities may be observed, and they appear at a random sequence. The red curve (with circle symbols) in Figs. 3(*a*) and

3(*b*) shows the cases where finger occurs prior to cavitation, and the blue curve (with triangle symbols) in Figs. 3(*a*) and 3(*c*) shows the cases of the opposite sequence. As shown in Fig. 3(*b*), when the adhesive layer is stretched to about $\lambda = 1.6$, the layer suffers fingering instability first. Under further stretch, a cavity emerges suddenly, accompanied by a small drop in stress, corresponding to images a2 and a3. Then the cavitation and fingers coexist until the entire layer fractures (image a5). In another case, as shown in Fig. 3(*c*), cavitation arises before the fingering instability. Different from the sudden appearance of cavity in Fig. 3(*b*), the cavity grows gradually when the adhesive layer is further loaded. Even though the experimental conditions are the same, different instability behaviors are observed. This phenomenon will be discussed further in Sec. 4. For an adhesive layer with a relatively large aspect ratio, both types of instabilities appear during the deformation. By partitioning the adhesive layer into smaller parts, which relax lateral constraints, the cavitation instability can be suppressed, and the mechanical responses of a partitioned adhesive layer are similar to the ones with smaller aspect ratios.

Cyclic loading is common when the adhesive layers are used for adhesion or as soft joints. Here, we study the effect of partition number on the mechanical responses to cyclic loading and present the results in Fig. 4. The adhesive layers (aspect ratio $\alpha = 12$) are loaded to a given stretch, followed by a complete unloading to the original thickness, and such a process is repeated for 10 times on each sample. For all adhesive layers, with or without partitioning, the first loading curve is always higher than the following ones due to the Mullins effect [31]. The second loading curve appears to be softer than the first one, as some polymer chains suffer irreversible damage. If the maximum strains in subsequent cycles do not exceed the first one, no new damage is made, and the curves change only slightly from the second to the tenth cycle. When the number of partitions increases, the area of the hysteresis loop decreases gradually. (The areas of the hysteresis loops are 2.38 KJ/m^3, 1.40 KJ/m^3, 1.28 KJ/m^3 and 1.25 KJ/m^3.) Increasing the number of partitions of the soft adhesive layers reduces the lateral confinement and hence decreases the area of the hysteresis loop.

Besides changing the number of partitions, another method of adjusting the mechanical responses of an adhesive layer is to change the length of the partition divider. As shown in Fig. 5, with the number of the partitions fixed as four and the radius of the layer as 15 mm, we change the divider length from 5 mm, 10 mm to 15 mm. When the length of divider increases, the stress–stretch curve changes from nonmonotonic to a monotonic one, the stress at the same stretch decreases significantly, and the layer becomes more stretchable compared to the original one, similar to the

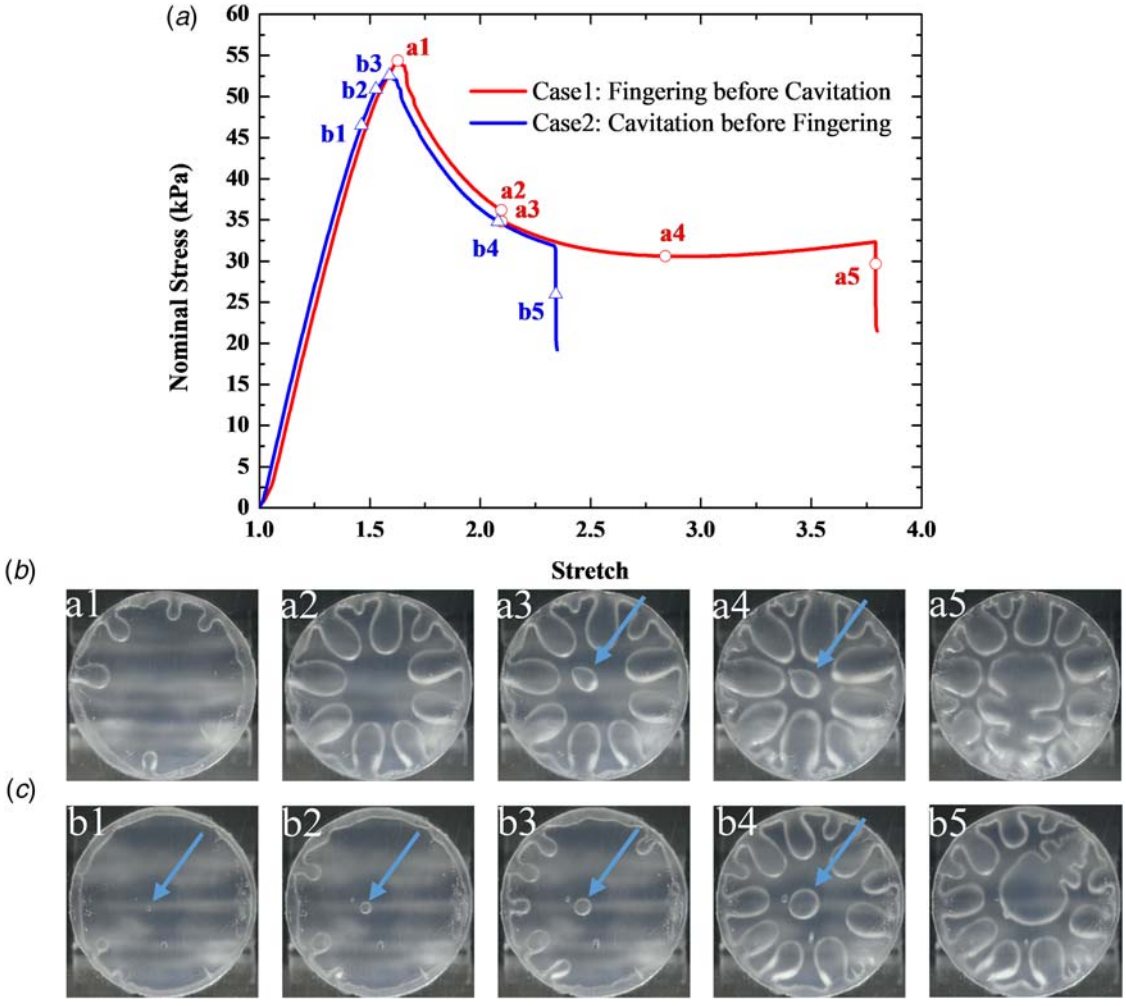

Fig. 3 Coexistence of fingering instabilities and cavitation in adhesive layers of aspect ratio ($\alpha = 20$), without partitioning. (*a*) Nominal stress–stretch curve in the case when fingering appears before cavitation (the red curve with circle symbols). Fingers appear at point a1, and a cavity appears later at point a2. Nominal stress–stretch curve in the case when cavitation appears before fingering (the blue line with triangle symbols). A visible cavity can be spotted at point b1. On further stretching, the cavity grows gradually and fingers emerge around point b2 or b3. (*b*) and (*c*) Photographs taken from the bottom of the adhesive layers corresponding to the indicated points on the nominal stress–stretch curves. (see color figure online)

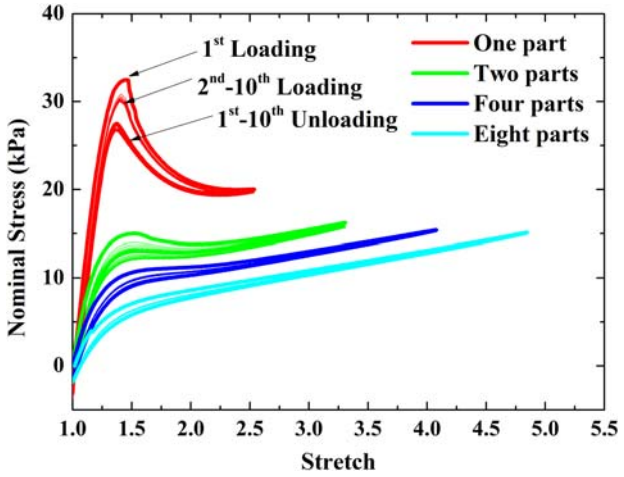

Fig. 4 Nominal stress–stretch curves of adhesive layers ($\alpha = 12$) under cyclic tests with various numbers of partitions. The first loading curve is always higher than the following loading curves due to the Mullins effect, and hysteresis loops exist between the loading and the unloading curves. As the number of partitions increases, the area of the hysteresis loop decreases.

changes in response to the increase in number of partitions as shown in Fig. 2. According to Fig. 5(*b*), it is obvious that for adhesive layers with LP (length of partition divider) = 5 mm or LP = 10 mm, the fracture stretches, and the fracture works are larger than those of adhesive layers with LP = 15 mm. It seems that there is an optimal length of partition divider, which corresponds to the maximal fracture stretch or the maximal fracture work, the optimal solution of length of partition is out of the scope of this paper.

4 Discussion

The slight reduction in the cross-sectional area aside, the main reason for the softening of the adhesive layer by partitioning is the reduction in lateral constraints. For an adhesive layer of the same thickness, a smaller partition has a smaller aspect ratio, and the deformation is closer to that in unconstrained uniaxial tension [20].

Let λ_c denote the critical stretch at which fingering instability appears within the adhesive layer without partition and S_c denote the nominal stress at stretch λ_c. From experiments, the S_{c1} for adhesive layer ($\alpha = 12$) without partitioning is 32 kPa, while the S_{c8} for adhesive layer ($\alpha = 12$) partitioned into eight parts is 6 kPa, indicating that partitioning plays an important role on softening the adhesive layer.

As mentioned earlier, the appearance order of cavitation and fingering instability is uncertain for an adhesive layer with the large

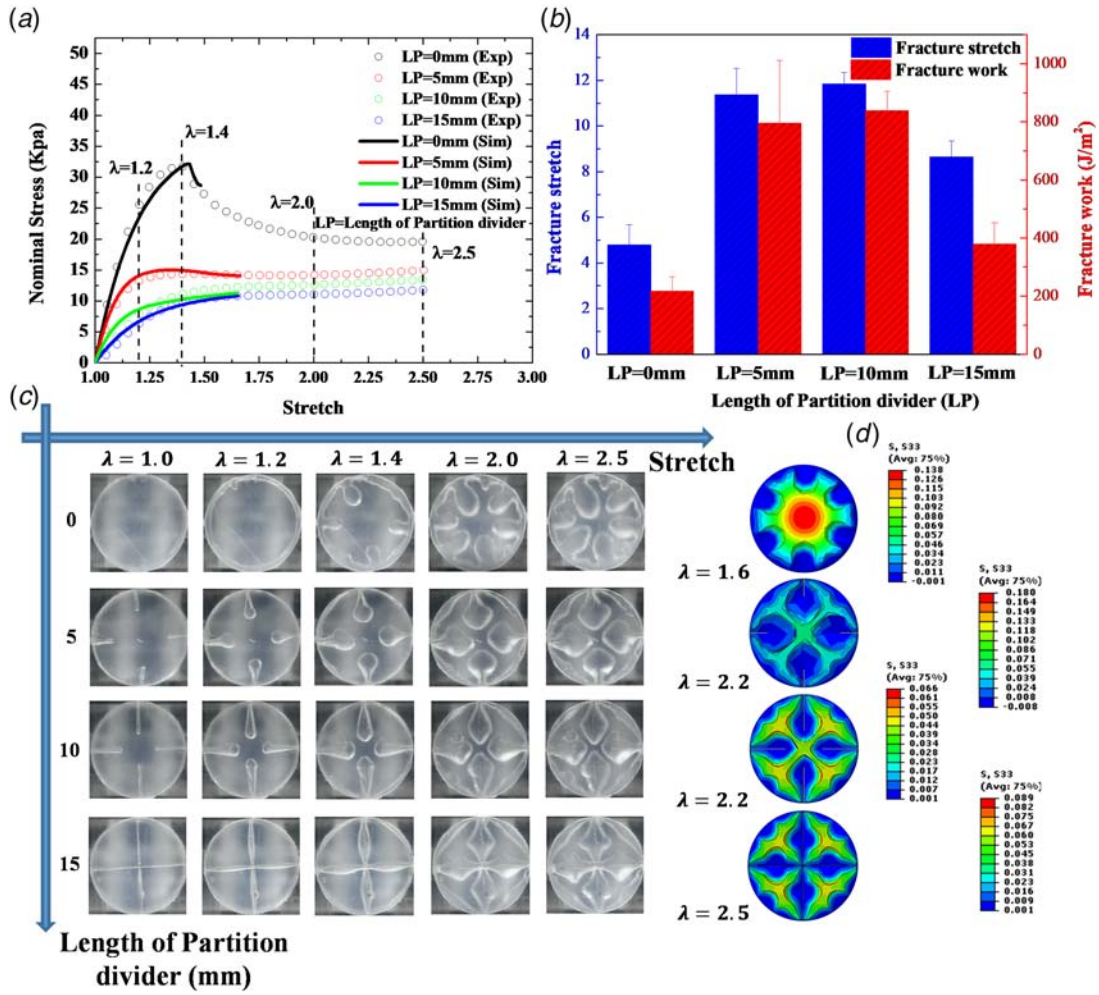

Fig. 5 Mechanical responses of soft adhesive layers ($\alpha = 12$) with partition dividers of various lengths. (*a*) Nominal stress–stretch curves of the adhesive layers. The circles are obtained from experiments, and the solid curves from simulations. (*b*) Fracture stretches and fracture works of the adhesive layers with partition dividers of various lengths. (*c*) Photographs taken from the bottom of the adhesive layers corresponding to the indicated stretches in (*a*). (*d*) Simulated instability morphologies for the cases with dividers of various lengths.

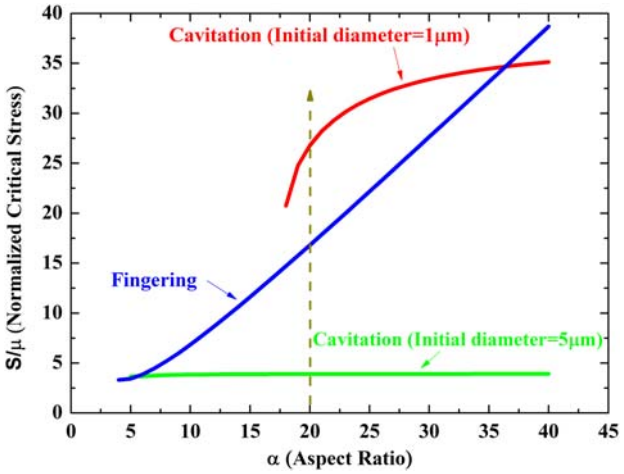

Fig. 6 Normalized critical stress versus aspect ratio for fingering instability and cavitation. The red (upper) and green (lower) lines correspond to the unstable growth of cavities with initial diameters of 1 μm and 5 μm, respectively. For an adhesive layer of an aspect ratio $\alpha = 20$, the critical stress for fingering is larger than that for cavitation with a bigger initial defect (e.g., 5 μm), but smaller than the cavitation stress for a smaller initial defect (e.g., 1 μm). (see color figure online)

aspect ratio. We attribute this phenomenon to the existence of random defects in the adhesive layers. Following Lin et al. [12], the dimensionless critical stresses (normalized by the initial shear modulus) for the fingering instability and cavitation (elastic instability limit of cavity) are plotted in Fig. 6, as functions of the aspect ratio of a cylindrical soft layer, at two initial cavity diameters. When the initial diameter of the cavity R_0 is relatively large, or the dimensionless capillary number $\beta = \gamma/(\mu R_0)$ is small, the cavity instability takes place under a low stress level and shows negligible dependence on the lateral constraint. Here, μ is the shear modulus. While for the initial defects with a small diameter (or a large β), larger nominal stress is needed. In our experiment, the initial size of the defects in the hydrogel adhesive layer is randomly distributed for different specimen, resulting in random β. For relatively large defects, the critical nominal stress is lower than the stress needed for fingering instability. Accordingly, cavitation instability arises before fingering instability. On the other hand, for small defects, the critical cavitation stress can be larger than that for the fingering instability, and hence, fingers may appear first.

We should point out that the peak stress for cavitation in the above model is an elastic instability limit for neo-Hookean material with an initial cavity of micron size [21]. Furthermore, the surface energy constant in the model is assumed to be deformation independent. Conversely, because of the inverse dependence of the peak stress on the cavity size, a material with very small cavities may experience material failure at a smaller stress level than the elastic instability limit.

For various applications, different properties of the adhesive layers are required. When the adhesive layer is used as a superglue, high adhesion strength is required while the stretchability is not essential, so that a nonpartitioned layer is preferred. When the adhesive layer severs the purpose of a soft joint, cavitation should be avoided because the cavity expands and leads to the failure of the adhesive layer at a relatively small stretch [32]. Partitioning the soft adhesive layer can suppress cavitation instability by reducing the hydrostatic stress in the bulk. In other applications, such as tissue stitching, a softer adhesive layer is preferred to provide a larger displacement. As Li et al. [33] mentioned in their work, both strong interface adhesion and large deformability are essential when connecting tissues and deformable devices. By partitioning the adhesive layer with certain numbers or length of partition dividers, the lateral confinement reduces and fracture stretch increases, and hence, the layer can accommodate larger deformation. In this work, the effect of material properties on instabilities and mechanical responses adjustment of the soft adhesive layers is not involved. Recently, Lin et al. [34] pointed out that the material-stiffening could suppress fingering and fringe instabilities and alter mechanical responses. By combining the present method with suitable materials, one can achieve extensive adjustments on the mechanical responses of the adhesive layers.

5 Conclusions

We have demonstrated a method to adjust the mechanical responses of confined soft adhesive layers under tensile loading: partitioning the layers with different numbers and/or lengths of partition dividers. Through this approach, the following results can be achieved. First, the compliance and stretchability of the layer increase and the cavitation instability may be suppressed. Second, the stress–stretch curve can be adjusted from a nonmonotonic one to a monotonic one, so that the snap-through phenomenon can be avoided in force-controlled scenarios. Third, partitioning the layer decreases the area of the hysteresis loop under cyclic loading. The present method may provide guidelines for the design of soft adhesive layers for various applications.

Acknowledgment

This work was supported by the National Natural Science Foundation of China (Nos. 11525210, 11621062, and 91748209), and the Fundamental Research Funds for the Central Universities.

References

[1] Liu, X., Tang, T.-C., Tham, E., Yuk, H., Lin, S., Lu, T. K., and Zhao, X., 2017, "Stretchable Living Materials and Devices With Hydrogel–Elastomer Hybrids Hosting Programmed Cells," Proc. Natl. Acad. Sci. U.S.A., **114**(9), pp. 2200–2205.
[2] Ahmed, G., and Ahmed, E., 2018, "On the Role of the Plaque Porous Structure in Mussel Adhesion: Implications for Adhesion Control Using Bulk Patterning," J. Appl. Mech., **85**(12), 121003.
[3] Creton, C., and Ciccotti, M., 2016, "Fracture and Adhesion of Soft Materials: A Review," Rep. Prog. Phys., **79**(4), 046601.
[4] Shull, K. R., 2002, "Contact Mechanics and the Adhesion of Soft Solids," Mater. Sci. Eng. R, **36**(1), pp. 1–45.
[5] Yuk, H., Lin, S., Ma, C., Takaffoli, M., Fang, N. X., and Zhao, X., 2017, "Hydraulic Hydrogel Actuators and Robots Optically and Sonically Camouflaged in Water," Nat. Commun., **8**, 14230.
[6] Ball, J. M., 1982, "Discontinuous Equilibrium Solutions and Cavitation in Nonlinear Elasticity," Philos. Trans. R. Soc. B, **306**, pp. 557–611.
[7] Lopez-Pamies, O., Idiart, M. I., and Nakamura, T., 2011, "Cavitation in Elastomeric Solids: I—A Defect-Growth Theory," J. Mech. Phys. Solids, **59**(8), pp. 1464–1487.
[8] Zimberlin, J. A., and Crosby, A. J., 2010, "Water Cavitation of Hydrogels," J. Polym. Sci. Part B Polym. Phys., **48**(13), pp. 1423–1427.
[9] Zimberlin, J. A., Sanabriadelong, N., Tew, G. N., and Crosby, A. J., 2007, "Cavitation Rheology for Soft Materials," Soft Matter, **3**(6), pp. 763–767.
[10] Long, R., and Hui, C. Y., 2010, "Effects of Triaxiality on the Growth of Crack-Like Cavities in Soft Incompressible Elastic Solids," Soft Matter, **6**(6), pp. 1238–1245.
[11] Overvelde, J. T. B., Dykstra, D. M. J., de Rooij, R., Weaver, J., and Bertoldi, K., 2016, "Tensile Instability in a Thick Elastic Body," Phys. Rev. Lett., **117**(9), 094301.
[12] Lin, S., Mao, Y., Radovitzky, R., and Zhao, X., 2017, "Instabilities in Confined Elastic Layers Under Tension: Fringe, Fingering and Cavitation," J. Mech. Phys. Solids, **106**, pp. 229–256.
[13] Crosby, A. J., Shull, K. R., Lakrout, H., and Creton, C., 2000, "Deformation and Failure Modes of Adhesively Bonded Elastic Layers," J. Appl. Phys., **88**(5), pp. 2956–2966.
[14] Lin, S., Cohen, T., Zhang, T., Yuk, H., Abeyaratne, R., and Zhao, X., 2016, "Fringe Instability in Constrained Soft Elastic Layers," Soft Matter, **12**(43), pp. 8899–8906.
[15] Chung, J. Y., and Chaudhury, M. K., 2005, "Soft and Hard Adhesion," J. Adhes., **81**(10–11), pp. 1119–1145.
[16] Chakrabarti, A., and Chaudhury, M. K., 2013, "Direct Measurement of the Surface Tension of a Soft Elastic Hydrogel: Exploration of Elastocapillary Instability in Adhesion," Langmuir, **29**(23), pp. 6926–6935.
[17] Chaudhury, M. K., Chakrabarti, A., and Ghatak, A., 2015, "Adhesion-Induced Instabilities and Pattern Formation in Thin Films of Elastomers and Gels," Eur. Phys. J. E, **38**(7), pp. 1–26.

[18] Animangsu, A. G., and Chaudhury, M. K., 2003, "Adhesion-Induced Instability Patterns in Thin Confined Elastic Film," Langmuir, **19**(7), pp. 2621–2631.
[19] Webber, R. E., Shull, K. R., Roos, A., and Creton, C., 2003, "Effects of Geometric Confinement on the Adhesive Debonding of Soft Elastic Solids," Phys. Rev. E, **68**(1), 021805.
[20] Shull, K. R., and Creton, C., 2004, "Deformation Behavior of Thin, Compliant Layers Under Tensile Loading Conditions," J. Polym. Sci. Part B: Polym. Phys., **42**(22), pp. 4023–4043.
[21] Dollhofer, J., Chiche, A., Muralidharan, V., Creton, C., and Hui, C. Y., 2004, "Surface Energy Effects for Cavity Growth and Nucleation in an Incompressible Neo-Hookean Material—Modeling and Experiment," Int. J. Solids Struct., **41**(22–23), pp. 6111–6127.
[22] Gent, A. N., and Lindley, P. B., 1959, "Internal Rupture of Bonded Rubber Cylinders in Tension," Proc. R. Soc. Lond., **249**(1257), pp. 195–205.
[23] Chiche, A., Dollhofer, J., and Creton, C., 2005, "Cavity Growth in Soft Adhesives," Eur. Phys. J. E, **17**(4), pp. 389–401.
[24] Biwa, S., 2006, "Cavitation in Finite Elasticity With Surface Energy Effects," Int. J. Non-Linear Mech., **41**(9), pp. 1084–1094.
[25] Fond, C., 2001, "Cavitation Criterion for Rubber Materials: A Review of Void-Growth Models," J. Polym. Sci. Part B Polym. Phys., **39**(17), pp. 2081–2096.
[26] Pourmodheji, R., Qu, S., and Yu, H., 2018, "Two Possible Defect Growth Modes in Soft Solids," J. Appl. Mech., **85**(3), 031001.
[27] Shull, K. R., Flanigan, C. M., and Crosby, A. J., 2000, "Fingering Instabilities of Confined Elastic Layers in Tension," Phys. Rev. Lett., **84**(14), pp. 3057–3060.
[28] Biggins, J. S., Saintyves, B., Wei, Z., Bouchaud, E., and Mahadevan, L., 2013, "Digital Instability of a Confined Elastic Meniscus," Proc. Natl. Acad. Sci. U.S.A., **110**(31), pp. 12545–12548.
[29] Saintyves, B., Dauchot, O., and Bouchaud, E., 2013, "Bulk Elastic Fingering Instability in Hele-Shaw Cells," Phys. Rev. Lett., **111**(4), pp. 2466–2472.
[30] Mao, G., Wu, L., Liang, X., and Qu, S., 2017, "Morphology of Voltage-Triggered Ordered Wrinkles of a Dielectric Elastomer Sheet," J. Appl. Mech., **84**(11), 111005.
[31] Diani, J., Fayolle, B., and Gilormini, P., 2009, "A Review on the Mullins Effect," Eur. Polym. J., **45**(3), pp. 601–612.
[32] Cristiano, A., Marcellan, A., Long, R., Hui, C. Y., Stolk, J., and Creton, C., 2010, "An Experimental Investigation of Fracture by Cavitation of Model Elastomeric Networks," J. Polym. Sci. Part B Polym. Phys., **48**(13), pp. 1409–1422.
[33] Li, J., Celiz, A. D., Yang, J., Yang, Q., Wamala, I., Whyte, W., Seo, B. R., Vasilyev, N. V., Vlassak, J. J., and Suo, Z., 2017, "Tough Adhesives for Diverse Wet Surfaces," Science, **357**(6349), pp. 378–381.
[34] Lin, S., Mao, Y., Yuk, H., and Zhao, X., 2018, "Material-Stiffening Suppresses Elastic Fingering and Fringe Instabilities," Int. J. Solids Struct., **139–140**, pp. 96–104.